



Cite this: *Nanoscale*, 2024, **16**, 6507

Chemical transformation mechanism for blue-to-green emitting CsPbBr_3 nanocrystals[†]

Yuling Liu,^{‡,a,b,c} Rui Yun,^{‡,a,b,c} Yue Li,^{a,b,c} Wenda Sun,^{a,b,c} Tiancheng Zheng,^{a,b,c} Qian Huang,^{a,b,c} Libing Zhang  ^d and Xiyan Li  ^{*,a,b,c}

Recently, metal–halide perovskites have rapidly emerged as efficient light emitters with near-unity quantum yield and size-dependent optical and electronic properties, which have attracted considerable attention from researchers. However, the ultrafast nucleation rate of ionic perovskite counterparts severely limits the in-depth exploration of the growth mechanism of colloidal nanocrystals (NCs). Herein, we used an inorganic ligand nitrosonium tetrafluoroborate (NOBF_4) to trigger a slow post-synthesis transformation process, converting non-luminescent Cs_4PbBr_6 NCs into bright green luminescent CsPbBr_3 NCs to elucidate the concrete transformation mechanism *via* four stages: (i) the dissociation of pristine NCs, (ii) the formation of Pb–Br intermediates, (iii) low-dimensional nanoplatelets (NPLs) and (iv) cubic CsPbBr_3 NCs, corresponding to the blue-to-green emission process. The desorption and reorganization of organic ligands induced by NO^+ and the involvement of BF_4^- in the ligand exchange process played pivotal roles in this dissolution–recrystallization of NCs. Moreover, controlled shape evolution from anisotropic NPLs to NCs was investigated through variations in the amount of NOBF_4 . This further validates that additives exert a decisive role in the symmetry and growth of nanostructured perovskite crystals during phase transition based on the ligand-exchange mechanism. This finding serves as a source of inspiration for the synthesis of highly luminescent CsPbBr_3 NCs, providing valuable insights into the chemical mechanism in post-synthesis transformation.

Received 16th October 2023,
Accepted 26th February 2024

DOI: 10.1039/d3nr05215j
rsc.li/nanoscale

Introduction

Metal–halide perovskites (MHPs), which are ideal for next-generation light emitters, have drawn substantial interest in a number of optoelectrical applications such as high-definition displays, field-effect transistors and wearable electronics.^{1–7} Especially, major advances have been made in multicolor perovskite light-emitting diodes in terms of desired emission wavelengths, solution processing characteristics and the exceptional balance of cost and performance. Different from conventional nanocrystals (NCs) with covalent bonds and rigid crystal structures, MHP-NCs with soft lattices are primarily bound by ionic chemical bonds. The difference in binding strength

results in MHP-NCs having low lattice formation energy, high lattice ionicity, and sub-second formation kinetics. These properties make it challenging to stabilize MHP-NCs at small sizes and understand the mechanism of their dynamic growth *via* direct synthesis methods, which is critical for further optimizing the performance of MHP NCs. Therefore, it is necessary to explore some tactics to retard the nucleation and growth rate of nanocrystals to investigate the specific crystal growth kinetics. Tian's group devised a stepwise synthesis method triggered by a polar alcohol to control the reaction rate and analyze the formation process of CsPbBr_3 NCs.⁸ Li *et al.* developed a microwave-irradiation-assisted method to obtain intermediate products during the growth of CsPbBr_3 NCs.⁹ These studies provide useful insights into the formation mechanism of CsPbBr_3 NCs. However, the improvement of emission properties in the above-mentioned studies was not satisfactory and PLQYs were not high enough owing to the polar solvent and surface defects.

In addition, the noncovalent and high dynamic binding of surface capping ligands result in their easy desorption from the surface of NCs and further destabilize the morphology and crystal structure of pristine NCs.^{10–14} Nonetheless, this unique characteristic also presents an opportunity to achieve novel morphologies or different crystal phases through post-treat-

^aInstitute of Photoelectronic Thin Film Devices and Technology, Solar Energy Conversion Center, Nankai University, Tianjin 300350, P. R. China

^bKey Laboratory of Efficient Utilization of solar energy of Tianjin, Tianjin 300071, P. R. China

^cEngineering Research Center of Thin Film Photoelectronic Technology of Ministry of Education, Tianjin 300350, P. R. China. E-mail: xiyan.li@nankai.edu.cn

^dTianjin Key Laboratory of Molecular Optoelectronic, Department of Chemistry, Tianjin University, Tianjin, 300072, P. R. China

[†] Electronic supplementary information (ESI) available. See DOI: <https://doi.org/10.1039/d3nr05215j>

[‡] Equally contributed author.

ment. Thus, chemical transformation from zero-dimensional (0D) Cs_4PbBr_6 NCs to three-dimensional (3D) CsPbBr_3 NCs with desired optical properties has been proven to be a feasible and interesting method.^{15–17} Recent studies suggest that phase transition in a solution is easily generated by the stripping of CsBr or the insertion of excess PbBr_2 , while the 0D and 3D phases maintain a similar size distribution.^{18–20} Instead, Baranov *et al.* proposed a different post-synthetic strategy of converting oleylamine (OAm)/oleate (OA)-capped Cs_4PbBr_6 NCs into strongly emissive polymer-capped CsPbBr_3 NCs using poly(maleic anhydride-*alt*-1-octadecene) (PMAO). Due to the mild reactivity of the organic polymer, the intermediate Cs_4PbBr_6 – CsPbBr_3 heterostructures were monitored during a slow transformation process. The partially converted particles were obtained by the reaction of the succinic anhydride units of PMAO and OAm ligands bound to the surface of Cs_4PbBr_6 NCs.²¹ Such nanoscale transformation proves that this reaction is driven by the reactivity of the regents, opening up strategies for designing and precisely controlling the crystal growth at the nanoscale.

In this regard, the adsorption and desorption of ligands on the surfaces of NCs are crucial for the post-synthesis transformation of their morphology and the crystallographic phase. Introducing new additives to as-prepared MHP-NCs can not only alter their surface properties but also trigger the post-synthesis transformation, leading to morphology evolution and crystallographic phase transition of NCs.^{22–25} Inorganic ligand (nitrosonium tetrafluoroborate, NOBF_4) is applicable for surface modification with nanoparticles (*e.g.*, NaYF_4 , Fe_3O_4 , TiO_2 , FePt and Bi_2S_3).^{26–30} Sequential surface functionalization of colloidal nanomaterials can be achieved without altering their size and shape. This process replaces the hydrophobic ligands on the NCs' surface with short-chain ligands, making the nanoparticles accessible for various applications in biology, photovoltaics and other fields. Very recently, we have reported an inorganic ligand (NOBF_4) mediated transform-

ation strategy from non-luminescent Cs_4PbBr_6 NCs to the precisely controllable blue-emitting CsPbBr_3 NPLs with a two-monolayer (2 ML) unit cell.³¹ This treatment revealed a dynamic dissolution–recrystallization process along with the appearance of deep-blue light (444 nm), where the nitrite ion (NO^+) rendered the intrinsic Cs_4PbBr_6 NCs unstable by stripping the organic species from their surface. Meanwhile, the NO^+ -induced acidic environment can protonate OAm into OAm^+ cations, thus enabling the slow precipitation of the precisely controllable 2 ML CsPbBr_3 NPLs in the non-polar solvent (several hours).

Herein, we will extend our investigation by studying the influence of the content of dissociating agent NOBF_4 on the Cs_4PbBr_6 NCs. Benefiting from the non-polar environment, the reaction process with different amounts of NOBF_4 was monitored by time-dependent photoluminescence (PL) and absorption spectra due to a slow reaction rate. We found that the shape of the products was controllable from the anisotropic NPLs to bulk CsPbBr_3 NCs by increasing the amount of NOBF_4 , accompanied by the slow transformation of blue into green light in the solution, corresponding to several specified emissions (Fig. 1, and S1†). More details on the conversion mechanism and surface capping properties were explored carefully by detecting the intermediate products during the phase transition process from non-luminescent Cs_4PbBr_6 NCs into brightly green luminescent CsPbBr_3 NCs. It was noted that the ligand desorption depended on the amount of NO^+ , while BF_4^- also participated in the ligand exchange process and was adsorbed on the surface of the reconstructed crystal. In addition, the fully-transformed CsPbBr_3 NCs exhibited a narrow emission line width of 18 nm and high photoluminescence quantum yield in the solution (up to 80%). Thus, this post-processing provides valuable insight into the mechanism of crystal growth and has potential application in the synthesis of highly luminescent NCs.

Results and discussion



Xiyian Li

Xiyian Li is currently a full professor in the College of Electronic Information and Optical Engineering at Nankai University of China. She received her Ph.D. degree from Changchun Institute of Applied Chemistry, Chinese Academy of Sciences in 2013. She then worked as a post-doctoral fellow at National University of Singapore from 2013 to 2015, and at the University of Toronto from 2015 to 2019, respectively. Her current research focuses on the controlled synthesis, novel properties, and optoelectronic applications of semiconductor nanostructures, especially perovskite-based optoelectronic devices.

research focuses on the controlled synthesis, novel properties, and optoelectronic applications of semiconductor nanostructures, especially perovskite-based optoelectronic devices.

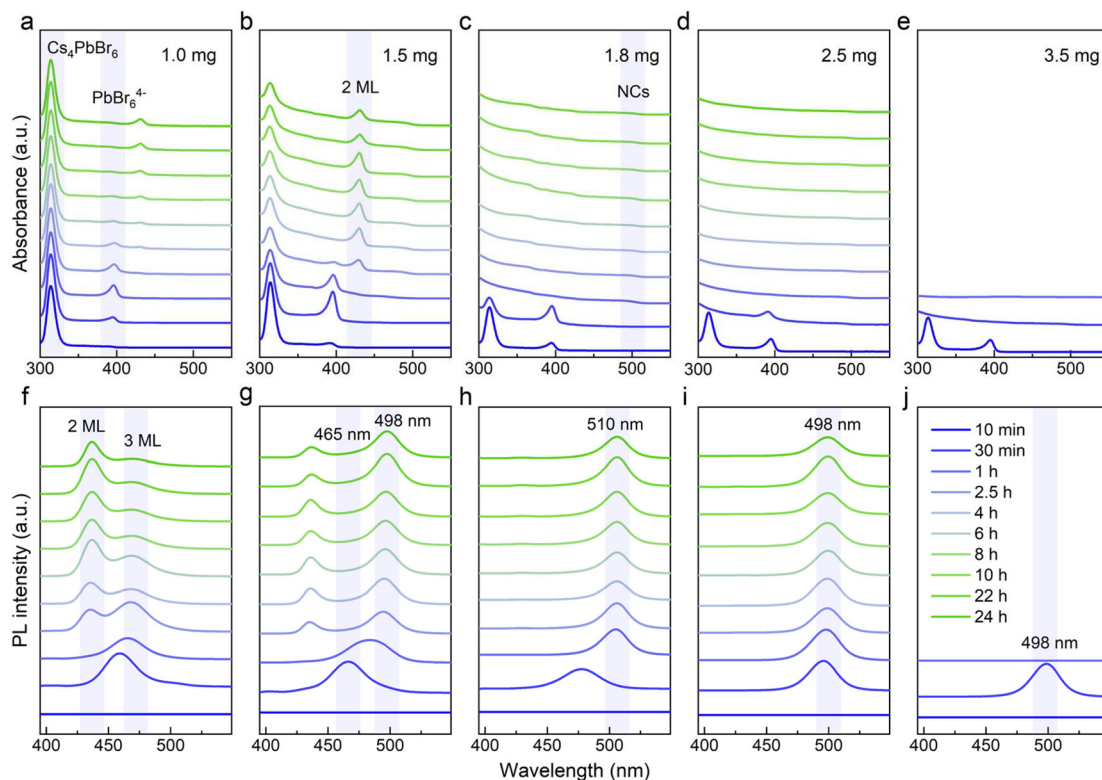


Fig. 1 (a–e) Absorption and (f–j) PL spectra of luminescent products obtained with different amounts of NOBF_4 (1.0 mg, 1.5 mg, 1.8 mg, 2.5 mg and 3.5 mg) at different reaction times.

corresponding to the obvious change in the luminescent color under the ambient light (left) as well as 365 nm UV irradiation (right) (Fig. S1†). It was worth noting that the multiple strong absorption and emission bands observed in the evolutionary spectra were similar to those from the previous reports, which were identified as the characteristic peaks of the 0D Cs_4PbBr_6 , Pb–Br intermediates, low-dimensional CsPbBr_3 NPLs (2 ML and 3 ML) and 3D CsPbBr_3 NCs.^{31,32} Hence, it is reasonable to speculate that these intermediate processes were closely related to the final precipitation of the brightly green-emitting MHP-NCs. In order to clarify the chemical transformation mechanism for this blue-to-green emitting perovskite analogous, we recorded the time-dependent absorption and photoluminescence (PL) spectra in detail over a long period of time. In Fig. 1a and b, it was found that the excitonic absorption band at 314 nm of Cs_4PbBr_6 NCs co-existed with Pb–Br intermediates (396 nm) or 2 ML anisotropic NPLs (430 nm) because the intrinsic Cs_4PbBr_6 NCs in the crude solution could not be completely consumed when the additive content was below 1.5 mg. As shown in Fig. 1f and g, we also monitored the 2 ML (436 nm) to 3 ML (468 nm) NPLs and 3 ML NPLs (465 nm) to 3D CsPbBr_3 NCs (498 nm) transformation process in PL evolution along with the residual intermediates (436-to-468 nm and 465-to-498 nm). Especially, the characteristic peak of 3 ML NPLs within 30 minutes always appears first, that is, the long-wavelength products in the dual-emission prefer to precipitate, reflecting that the conversion of intermediates was easier than its formation.

When the additive was sufficient, the characteristic absorption peak of the original Cs_4PbBr_6 NCs at 314 nm and PbBr_6^{4-} octahedra at 396 nm gradually disappeared accompanied by the emergence of a new peak at approximately 497 nm after 30 minutes, assigned to CsPbBr_3 NCs (Fig. 1c and d). The corresponding emission shape was a single green-emitting band around 500 nm (Fig. 1h and i). It was seen that the additive amount of 1.8 to 2.5 mg was just in the range of 0D-to-3D complete conversion (Fig. 1c, d, and h, i). Notably, the minor differences in the additive content led to the final emission position shifting to a shorter wavelength (from 510 nm to 498 nm, Fig. 1h and i), which may be due to the etching effect of the nitrite ion.^{26,31} From Fig. 3b and d, it was found that the quantum yield (QY) of the conversion products increases dramatically within four hours and was gradually stabilized at approximately 80%. In Fig. 3c and e, the time-resolved PL measurements reflected the average lifetimes of these CsPbBr_3 NCs ranging from 4.10 to 5.50 ns (Tables S1, and S2†).^{33,34}

As the additive increases to 3.5 mg, the initially observed green light appearing within 30 minutes, rapidly diminished due to an intensified attack by the nitrite ion on the perovskite counterparts in the non-polar solvent. Meanwhile, it was noted that the non-luminescent impurities of CsBF_4 and $(\text{CsF})\text{Br}_2$ phases were formed (Fig. S3†). Through the above analysis, we conclude that the intrinsic Cs_4PbBr_6 NCs underwent a dissociation–recrystallization process, where the free ions first aggregate to form the Pb–Br octahedra, and then grow from 2

ML to 3 ML and eventually into CsPbBr_3 NCs, accompanied with the color evolution from deep blue (~ 436 nm) to pure blue (~ 468 nm) and finally green emitting (~ 500 nm). The NOBF_4 concentration and time-dependent chemical transformation process are summarized in Fig. 2.

The XRD patterns of the perovskite counterparts obtained at 15 min, 30 min, 1 h, 4 h, 8 h and 24 h are depicted in Fig. 3a, which agreed with the hexagonal Cs_4PbBr_6 (blue) and orthorhombic CsPbBr_3 (green) reference. As the reaction pro-

ceeded, it was noted that the 0D phase initially coexisted with the 3D phase, followed by a gradual decrease of the diffraction peak of Cs_4PbBr_6 . The periodic diffraction peak within 30 min further confirmed the existence of 2 ML NPLs in the early stage of the reaction, along with a stacking distance of 4.6 nm and a uniform thickness of the inorganic layer at 1.1 nm (Fig. S4†). As shown in Fig. 4, transmission electron microscopy (TEM) was employed to monitor the chemical transformation process. The small particles within 30 min were proven to be completely dissociated Cs_4PbBr_6 nanoparticles, as described in previous reports, gradually growing into white square particles, corresponding to the increased average size from 10.9 nm to 14.9 nm (Fig. S5, and 6†). Meanwhile, the size of partially dissolved Cs_4PbBr_6 nanoparticles slightly decreased (from 11.2 nm to 7.9 nm), indicating that the dissolution and recrystallization processes occurred simultaneously (Fig. S7†). The phase structure of white square particles was further identified by their lattice fringe in the HRTEM image, and the spacing of 0.29 nm corresponded to the (002) plane in CsPbBr_3 NCs (Fig. 4h).³⁵ Taken together, the sequential step growth was monitored optically and microscopically, evidenced by the possible growth mechanism of bulk CsPbBr_3 NCs along with their shape and phase transformation.

Currently, it is widely accepted that reaction temperature is crucial for the formation of anisotropic MHP-NPLs: by lowering the temperature it is possible to have an atomic-scale control over the thickness down to the few monolayers that are thin enough to exhibit the characteristics of quantum confine-

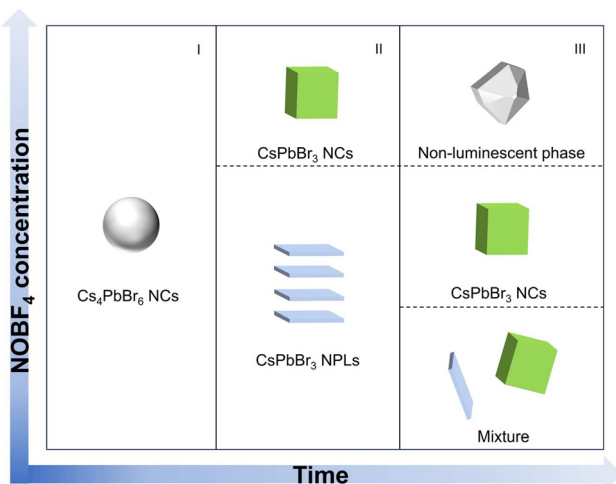


Fig. 2 Schematic presentation of the nanostructures in the reaction medium with the reaction time and NOBF_4 concentration.

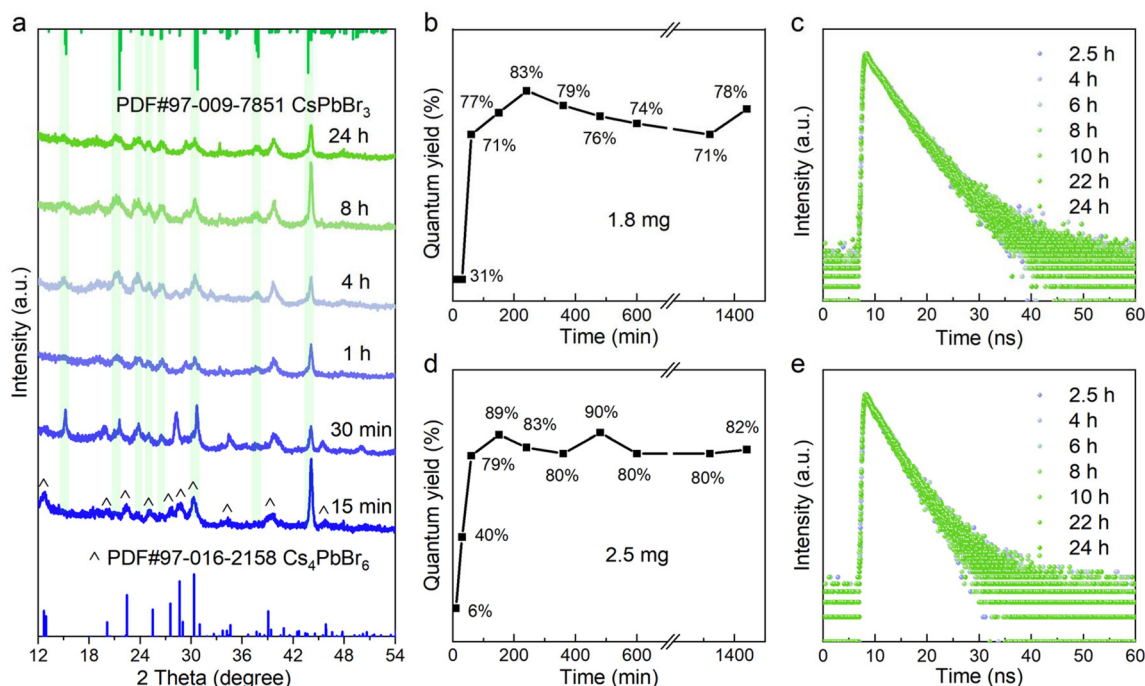


Fig. 3 (a) XRD patterns of the luminescent products synthesized with 1.8 mg NOBF_4 at different reaction times. (b and d) Quantum yield and (c and e) PL decay spectra of the luminescent products synthesized with 1.8 mg and 2.5 mg NOBF_4 at different reaction times.

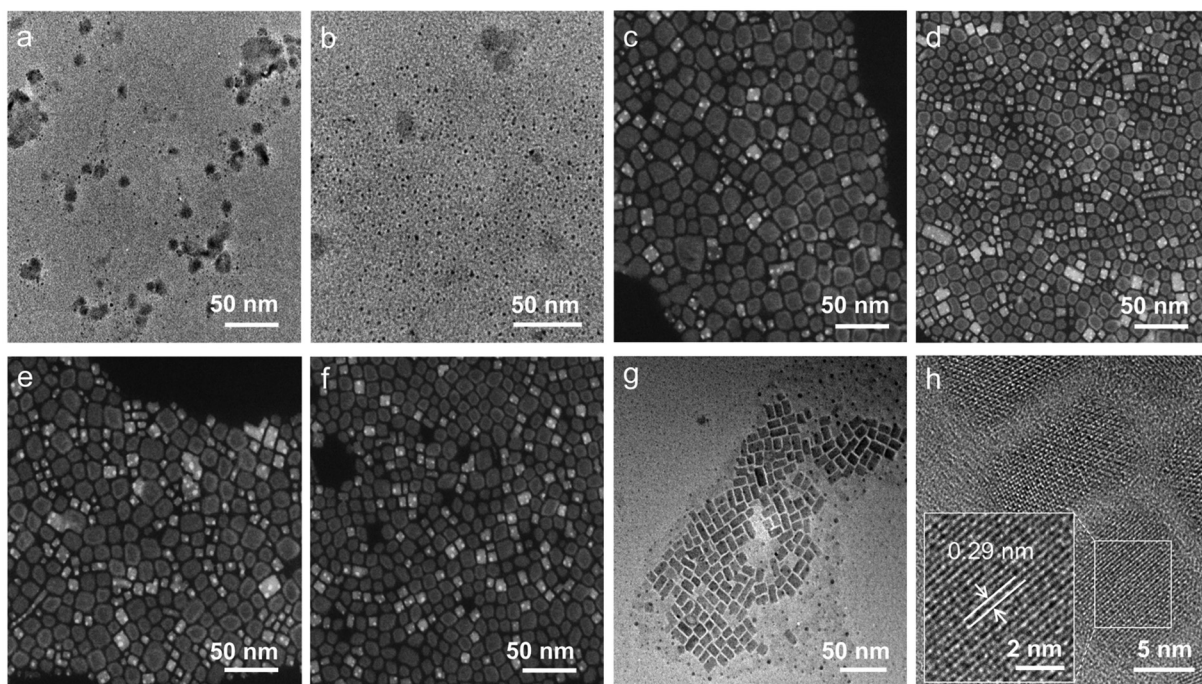


Fig. 4 (a–f) TEM images of the luminescent products obtained with 1.8 mg NOBF_4 at 15 min, 30 min, 1 h, 4 h, 8 h and 24 h. (g) TEM and (h) HRTEM images of the purified luminescent products obtained with 1.8 mg NOBF_4 .

ment.³⁶ Therefore, the question arises, how does this additive precisely control the lateral dimension of perovskite counterparts at the atomic-scale thickness? To address this, we conducted the Fourier transform infrared (FTIR) measurements on the pristine Cs_4PbBr_6 treated with/without NOBF_4 (Fig. 5a). After the NOBF_4 treatment, it was observed that a significant reduction occurred in the characteristic C–H stretching vibrations at $2800\text{--}3000\text{ cm}^{-1}$ and 1470 cm^{-1} , as well as the vibration of N–H bending at 1570 cm^{-1} . The band around 1710 cm^{-1} was assigned to the C=O stretching vibration of OA.³¹ These results indicated that a substantial number of ligands bound to the Cs_4PbBr_6 NCs surface were effectively eliminated since the nitrite ion in the additive was reactive towards amine species. Unlike the untreated sample, a new emerging peak at 1084 cm^{-1} , was identified to the BF_4^- anion.^{26,37} This phenomenon of BF_4^- anions adsorption on the surface is common in surface modification of various colloidal nanoparticles, but it was not observed in our previous studies on 2 ML blue-emitting NPLs.³¹ Moreover, no signal attributable to NO^+ was detectable in the region from 2100 to 2200 cm^{-1} .^{26,38} Therefore, we hypothesize that the surface capping properties of the sample treated with more additives were distinct from those reported previously for 2 ML NPLs.³¹

X-ray photoelectron spectroscopy (XPS) measurement was performed to analyze the surface binding ligands. The full XPS survey spectra of Cs_4PbBr_6 NCs (0 h) and CsPbBr_3 NCs (24 h) revealed the existence of Cs, Pb, Br, N, B and F (Fig. 5b), and the bonding information was investigated in detail by the high-resolution XPS. As shown in Fig. 5c, d and S8,† CsPbBr_3

NCs gradually shifted towards higher binding energies for Cs 3d, Pb 4f and Br 3d compared with the pristine Cs_4PbBr_6 NCs, demonstrating the stronger Pb–Br interactions in the $[\text{PbBr}_6]^{4-}$ octahedra. The signal of B 1s and F 1s were detected in CsPbBr_3 NCs (Fig. S8†); this observation aligned with the FTIR results, implying that a ligand-exchange process occurred between the organic ligands and inorganic BF_4^- anions. Moreover, for the treated samples, we observed that a dominant peak at 401.6 eV coexisted with the relatively weak peak at 399.8 eV in N 1s spectra (Fig. 5e), which were associated with the protonated amines ($-\text{NH}_3^+$) and $-\text{NH}_2$ groups of OAm, respectively.^{39,40} Compared to the reported organic species on the NPLs' surface, it was noted that partial $-\text{NH}_3^+$ was reduced to $-\text{NH}_2$ groups of OAm in the green-emitting nanocubes since the abundant nitrite ions in the system would cause a stronger surface etching for the Cs_4PbBr_6 nanoparticles and accelerate the fusion of NPLs through the bare-surface contact.⁴¹ Thus, we concluded that the nanoplatelet–nanocube ripening was driven by the additive-induced ligand desorption.

In previous studies, NOBF_4 was employed for surface modification based on a generalized ligand-exchange strategy in semiconductor and metal NC systems, allowing surface functionalization of nanoparticles and reversible phase transfer between hydrophobic and hydrophilic media without altering their size and shape. In principle, NO^+ was found to remove the native capping molecules adhered to the NC surface, and readily reacted with water molecules in the solvent to make the conditions acidic, while the weakly coordinated BF_4^- imparted a higher colloidal solubility for NCs

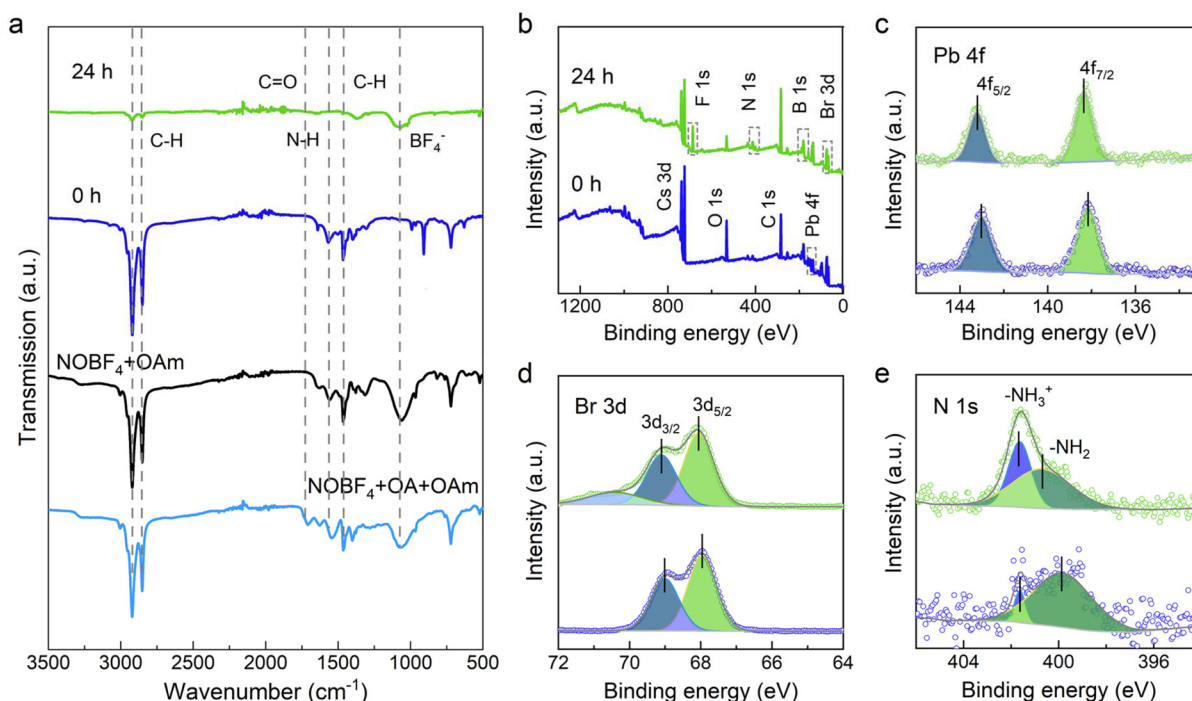


Fig. 5 (a) FTIR and (b) full XPS spectra of pristine Cs_4PbBr_6 NCs (0 h) and the newly formed CsPbBr_3 NCs after 24 h with 1.8 mg NOBF_4 . High-resolution XPS spectra of (c) Pb 4f, (d) Br 3d and (e) N 1s.

in polar solvents, especially for large-sized NCs.²⁶ For ionic MHP-NCs, it is extremely sensitive to tiny changes in the ligand species due to the significant influence of surface chemistry on the growth of nanoscale perovskite materials. Thus, the removal of amine ligands from the NC surface after adding NOBF_4 causes the pristine NCs to dissociate into free ions, and the surface ligand species are likely to undergo reassignment because the acidic protons turn OAm into OAm cations, as evidenced by our previous work. Benefiting from the non-polar solvent, the intrinsic growth and highly anisotropic crystal shape of the recrystallized perovskite counterparts can be engineered precisely at the atomic-level thickness. Such surface modification mechanism is also applicable to blue-green emitting MHP-NCs having a variety of sizes and shapes in this work.

The entire transformation process can be divided into four stages, as illustrated in Fig. 6, involving (i) the pristine 0D Cs_4PbBr_6 NCs dissociated into free ions after adding the inorganic ligand into the non-polar solvent; (ii) a series of Pb–Br intermediates formed initially when these ions are encountered; (iii) the presence of Cs^+ in the system along with the emerging protonated OAm ions were scrambling to fill the bromoplumbate ionic scaffold, accompanied by the appearance of deep-blue light with respect to the low-dimensional NPLs; (iv) as time goes on, a larger nanostructure was generated due to the NPLs losing strong quantum confinement following exposure to more additives, corresponding to slight ripening of nanoplatelets–nanocubes, that is the blue-emitting NPLs were consumed during the growth of larger and more stable

cube-like particles. It is well-established that the oriented attachment often appears in a wide variety of nanomaterials, in which these NPLs with identical crystallographic facets were stacked together and subsequently assembled into larger nanostructures with lower surface energy.^{36,41–43} Such an attachment process is driven by the ligand desorption with respect to the poor binding organic ligands. Accordingly, it was anticipated that some factors were able to accelerate the ligand desorption and thereby ripened NPLs to bulk nanostructures, such as temperature, polar solvents and light.^{44–46}

Based on the above analysis, we found that the amounts of the additives are essential for the emission color of final perovskite products, as depicted in Fig. 1. Following the increased NOBF_4 , it was noted that the number of layers of NPLs gradually increased in a sequence and the blue-green transformation process was promoted. The multiple emission peaks indicated that small amounts of additives are likely to capture the intermediate state of partially converted products as a full coalescence of 2D NPLs difficult to access for minor NO^+ . Moreover, this monitored slow transition process from low-dimensional NPLs revealed the dynamic growth kinetics of the bulk nanostructured CsPbBr_3 crystal. In addition, the PL properties of the green-emitting CsPbBr_3 NCs dispersed in a non-polar cyclohexane system were investigated to evaluate their environmental stability. As shown in Fig. S9a,† it always maintains good monochromaticity and its luminescence position has no obvious fluctuation after 12 days of storage in ambient atmosphere, and the FWHM remained constant at 18 nm (Fig. S9b†). The luminescence intensity decreased by 20%

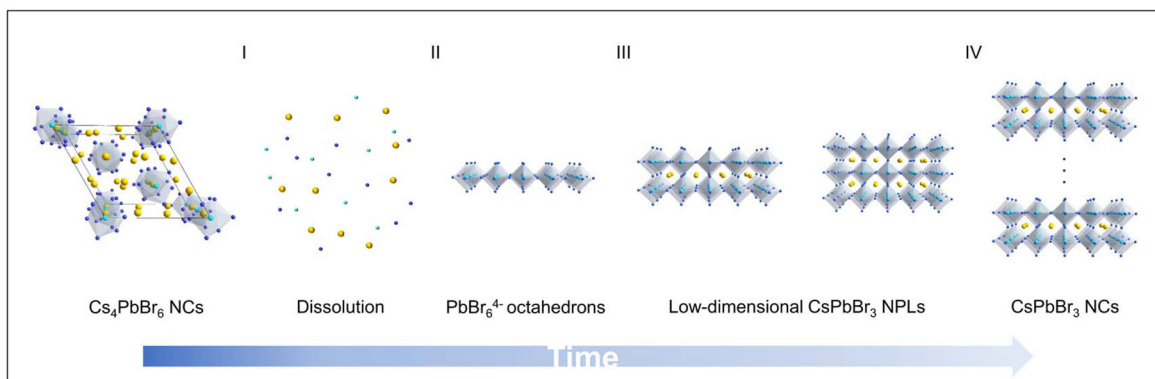


Fig. 6 Schematic illustration of the proposed transformation mechanism.

within two weeks (Fig. S9b†), which is related to the highly dynamic binding character of surface organic species. Overall, this approach not only synthesizes highly luminescent CsPbBr_3 NCs but also provides an effective pathway to understand the dynamic growth mechanism of MHP-NCs and precisely control their optical behavior.

Conclusion

In summary, we utilized the stripping effect of NO^+ as a dissociating agent to induce the chemical transformation from non-luminescent Cs_4PbBr_6 to bright green-emitting CsPbBr_3 . It was found that more additives accelerated the ligand desorption of the weakly binding capping molecules and facilitated the coalescence of NPLs into cube-like nanoparticles. This phenomenon corresponds to the noticeable characteristic redshifts in the absorption and PL spectra, portraying a comprehensive evolution in morphology and structure changes of the non-luminescent nanoparticles over 24 h. Interestingly, BF_4^- is also adsorbed onto the surface of the reconstructed nanocrystal to enrich its surface properties. This surface modification approach proves to be applicable to MHP-NCs, endowing them with various surface functionalizations to precisely engineer their surface properties.

Author contributions

Yuling Liu and Rui Yun: conceptualization, data curation, writing – original draft and writing – review. Yue Li: investigation. Wenda Sun and Tiancheng Zheng: formal analysis. Qian Huang and Libing Zhang: supervision and funding acquisition. Xiyan Li: supervision, funding acquisition, and final writing – review. All authors approved the final manuscript.

Conflicts of interest

There are no conflicts to declare.

Acknowledgements

This work was financially supported by the National Natural Science Foundation of China (Grant No. 22275101).

References

- 1 A. Dey, J. Ye, A. De, E. Debroye, S. K. Ha, E. Bladt, A. S. Kshirsagar, Z. Wang, J. Yin, Y. Wang, L. N. Quan, F. Yan, M. Gao, X. Li, J. Shamsi, T. Debnath, M. Cao, M. A. Scheel, S. Kumar, J. A. Steele, M. Gerhard, L. Chouhan, K. Xu, X. G. Wu, Y. Li, Y. Zhang, A. Dutta, C. Han, I. Vincon, A. L. Rogach, A. Nag, A. Samanta, B. A. Korgel, C. J. Shih, D. R. Gamelin, D. H. Son, H. Zeng, H. Zhong, H. Sun, H. V. Demir, I. G. Scheblykin, I. Mora-Sero, J. K. Stolarczyk, J. Z. Zhang, J. Feldmann, J. Hofkens, J. M. Luther, J. Perez-Prieto, L. Li, L. Manna, M. I. Bodnarchuk, M. V. Kovalenko, M. B. J. Roeffaers, N. Pradhan, O. F. Mohammed, O. M. Bakr, P. Yang, P. Muller-Buschbaum, P. V. Kamat, Q. Bao, Q. Zhang, R. Krahne, R. E. Galian, S. D. Stranks, S. Bals, V. Biju, W. A. Tisdale, Y. Yan, R. L. Z. Hoye and L. Polavarapu, State of the Art and Prospects for Halide Perovskite Nanocrystals, *ACS Nano*, 2021, **15**, 10775–10981.
- 2 R. Yun, H. Yang, W. Sun, L. Zhang, X. Liu, X. Zhang and X. Li, Recent Advances on Mn^{2+} -Doping in Diverse Metal Halide Perovskites, *Laser Photonics Rev.*, 2022, **17**, 2200524.
- 3 Q. Van Le, H. W. Jang and S. Y. Kim, Recent Advances toward High-Efficiency Halide Perovskite Light-Emitting Diodes: Review and Perspective, *Small Methods*, 2018, **2**, 1700419.
- 4 J. Chen, W. Du, J. Shi, M. Li, Y. Wang, Q. Zhang and X. Liu, Perovskite quantum dot lasers, *InfoMat*, 2019, **2**, 170–183.
- 5 P. Ramasamy, D. H. Lim, B. Kim, S. H. Lee, M. S. Lee and J. S. Lee, All-inorganic cesium lead halide perovskite nanocrystals for photodetector applications, *Chem. Commun.*, 2016, **52**, 2067.
- 6 X. Liu, D. Yu, X. Song and H. Zeng, Metal Halide Perovskites: Synthesis, Ion Migration, and Application in Field-Effect Transistors, *Small*, 2018, **14**, 1801460.

7 J. Zhao, L.-W. Lo, Z. Yu and C. Wang, Handwriting of perovskite optoelectronic devices on diverse substrates, *Nat. Photonics*, 2023, **17**, 964–971.

8 A. Liu, C. Bi, X. Qu and J. Tian, Demystifying the Formation of Colloidal Perovskite Nanocrystals via Controlling Stepwise Synthesis, *J. Phys. Chem. C*, 2021, **125**, 14204–14211.

9 Y. Li, H. Huang, Y. Xiong, S. V. Kershaw and A. L. Rogach, Revealing the Formation Mechanism of CsPbBr_3 Perovskite Nanocrystals Produced via a Slowed-Down Microwave-Assisted Synthesis, *Angew. Chem., Int. Ed.*, 2018, **57**, 5833–5837.

10 G. Almeida, L. Goldoni, Q. Akkerman, Z. Dang, A. H. Khan, S. Marras, I. Moreels and L. Manna, Role of Acid-Base Equilibria in the Size, Shape, and Phase Control of Cesium Lead Bromide Nanocrystals, *ACS Nano*, 2018, **12**, 1704–1711.

11 J. De Roo, M. Ibanez, P. Geiregat, G. Nedelcu, W. Walravens, J. Maes, J. C. Martins, I. Van Driessche, M. V. Kovalenko and Z. Hens, Highly Dynamic Ligand Binding and Light Absorption Coefficient of Cesium Lead Bromide Perovskite Nanocrystals, *ACS Nano*, 2016, **10**, 2071–2081.

12 Y. Bai, M. Hao, S. Ding, P. Chen and L. Wang, Surface Chemistry Engineering of Perovskite Quantum Dots: Strategies, Applications, and Perspectives, *Adv. Mater.*, 2022, **34**, 2105958.

13 F. Haydous, J. M. Gardner and U. B. Cappel, The impact of ligands on the synthesis and application of metal halide perovskite nanocrystals, *J. Mater. Chem. A*, 2021, **9**, 23419–23443.

14 S. R. Smock, T. J. Williams and R. L. Brutcher, Quantifying the Thermodynamics of Ligand Binding to CsPbBr_3 Quantum Dots, *Angew. Chem., Int. Ed.*, 2018, **57**, 11711–11715.

15 H. Yang, T. Cai, L. Dube, K. Hills-Kimball and O. Chen, Synthesis of Ultrathin Perovskite Nanowires via a Postsynthetic Transformation Reaction of Zero-Dimensional Perovskite Nanocrystals, *Cryst. Growth Des.*, 2021, **21**, 1924–1930.

16 A. Pramanik, S. Patibandla, Y. Gao, K. Gates and P. C. Ray, Water Triggered Synthesis of Highly Stable and Biocompatible 1D Nanowire, 2D Nanoplatelet, and 3D Nanocube CsPbBr_3 Perovskites for Multicolor Two-Photon Cell Imaging, *JACS Au*, 2021, **1**, 53–65.

17 S. Bera, R. K. Behera, S. D. Adhikari, A. K. Guria and N. Pradhan, Equilibriums in Formation of Lead Halide Perovskite Nanocrystals, *J. Phys. Chem. Lett.*, 2021, **12**, 11824–11833.

18 L. Wu, H. Hu, Y. Xu, S. Jiang, M. Chen, Q. Zhong, D. Yang, Q. Liu, Y. Zhao, B. Sun, Q. Zhang and Y. Yin, From Nonluminescent Cs_4PbX_6 ($X = \text{Cl}, \text{Br}, \text{I}$) Nanocrystals to Highly Luminescent CsPbX_3 Nanocrystals: Water-Triggered Transformation through a CsX -Stripping Mechanism, *Nano Lett.*, 2017, **17**, 5799–5804.

19 Q. A. Akkerman, S. Park, E. Radicchi, F. Nunzi, E. Mosconi, F. De Angelis, R. Brescia, P. Rastogi, M. Prato and L. Manna, Nearly Monodisperse Insulator Cs_4PbX_6 ($X = \text{Cl}, \text{Br}, \text{I}$) Nanocrystals, Their Mixed Halide Compositions, and Their Transformation into CsPbX_3 Nanocrystals, *Nano Lett.*, 2017, **17**, 1924–1930.

20 K. Xu, Q. Wei, H. Wang, B. Yao, W. Zhou, R. Gao, H. Chen, H. Li, J. Wang and Z. Ning, The 3D-structure-mediated growth of zero-dimensional Cs_4SnX_6 nanocrystals, *Nanoscale*, 2022, **14**, 2248–2255.

21 D. Baranov, G. Caputo, L. Goldoni, Z. Dang, R. Scarfiello, L. De Trizio, A. Portone, F. Fabbri, A. Camposeo, D. Pisignano and L. Manna, Transforming colloidal Cs_4PbBr_6 nanocrystals with poly(maleic anhydride-alt-1-octadecene) into stable CsPbBr_3 perovskite emitters through intermediate heterostructures, *Chem. Sci.*, 2020, **11**, 3986–3995.

22 S. Paul and S. Acharya, Postsynthesis Transformation of Halide Perovskite Nanocrystals, *ACS Energy Lett.*, 2022, **7**, 2136–2155.

23 N. Pradhan, Alkylammonium Halides for Facet Reconstruction and Shape Modulation in Lead Halide Perovskite Nanocrystals, *Acc. Chem. Res.*, 2021, **54**, 1200–1208.

24 L. Ruan, W. Shen, A. Wang, A. Xiang and Z. Deng, Alkyl-Thiol Ligand-Induced Shape- and Crystalline Phase-Controlled Synthesis of Stable Perovskite-Related CsPb_2Br_5 Nanocrystals at Room Temperature, *J. Phys. Chem. Lett.*, 2017, **8**, 3853–3860.

25 T. Udayabhaskararao, L. Houben, H. Cohen, M. Menahem, I. Pinkas, L. Avram, T. Wolf, A. Teitelboim, M. Leskes, O. Yaffe, D. Oron and M. Kazes, A Mechanistic Study of Phase Transformation in Perovskite Nanocrystals Driven by Ligand Passivation, *Chem. Mater.*, 2017, **30**, 84–93.

26 A. Dong, X. Ye, J. Chen, Y. Kang, T. Gordon, J. M. Kikkawa and C. B. Murray, A generalized ligand-exchange strategy enabling sequential surface functionalization of colloidal nanocrystals, *J. Am. Chem. Soc.*, 2011, **133**, 998–1006.

27 X. Lai, X. Li, X. Lv, Y.-Z. Zheng, F. Meng and X. Tao, Broadband dye-sensitized upconverting nanocrystals enabled near-infrared planar perovskite solar cells, *J. Power Sources*, 2017, **372**, 125–133.

28 J. Park, K. An, Y. Hwang, J.-G. Park, H.-J. Noh, J.-Y. Kim, J.-H. Park, N.-M. Hwang and T. Hyeon, Ultra-large-scale syntheses of monodisperse nanocrystals, *Nat. Mater.*, 2004, **3**, 891–895.

29 R. Malakooti, L. Cademartiri, Y. Akçakir, S. Petrov, A. Migliori and G. A. Ozin, Shape-Controlled Bi_2S_3 Nanocrystals and Their Plasma Polymerization into Flexible Films, *Adv. Mater.*, 2006, **18**, 2189–2194.

30 S. Sun, C. B. Murray, D. Weller, L. Folks and A. Moser, Monodisperse FePt Nanoparticles and Ferromagnetic FePt Nanocrystal Superlattices, *Science*, 2000, **287**, 1989–1992.

31 R. Yun, H. Yang, Y. Li, Y. Liu, Y. Chu, S. Wu, X. Liu, X. Zhang, L. Zhang and X. Li, Inorganic Ligand Triggered Transformation from Cs_4PbBr_6 Nanocrystals to Blue-Emitting CsPbBr_3 Nanoplatelets, *Chem. Mater.*, 2023, **35**, 424–431.

32 Y. Bekenstein, B. A. Koscher, S. W. Eaton, P. Yang and A. P. Alivisatos, Highly Luminescent Colloidal Nanoplates of Perovskite Cesium Lead Halide and Their Oriented Assemblies, *J. Am. Chem. Soc.*, 2015, **137**, 16008–16011.

33 H. Huang, W. Zhao, H. Yang, X. Zhang, J. Su, K. Hu, Z. Nie, Y. Li and J. Zhong, In situ synthesis of blue-emitting bromide-based perovskite nanoplatelets towards unity quantum efficiency and ultrahigh stability, *J. Mater. Chem. C*, 2021, **9**, 5535–5543.

34 J. Shamsi, D. Kubicki, M. Anaya, Y. Liu, K. Ji, K. Frohma, C. P. Grey, R. H. Friend and S. D. Stranks, Stable Hexylphosphonate-Capped Blue-Emitting Quantum-Confined CsPbBr_3 Nanoplatelets, *ACS Energy Lett.*, 2020, **5**, 1900–1907.

35 X. Xiao, Y. Li and R. J. Xie, Blue-emitting and self-assembled thinner perovskite CsPbBr_3 nanoplates: synthesis and formation mechanism, *Nanoscale*, 2020, **12**, 9231–9239.

36 N. T. Thanh, N. Maclean and S. Mahiddine, Mechanisms of nucleation and growth of nanoparticles in solution, *Chem. Rev.*, 2014, **114**, 7610–7630.

37 H. D. Lutz, J. Himmrich and M. Schmidt, Lattice vibration spectra. Part LXXXVI. Infrared and Raman spectra of baryte-type TiClO_4 , TiBF_4 , and NH_4BF_4 single crystals and of ^{11}B -enriched NH_4BF_4 , *J. Alloys Compd.*, 1996, **241**, 1–9.

38 T. Gerlach, F.-W. Schütze and M. Baerns, An FTIR Study on the Mechanism of the Reaction between Nitrogen Dioxide and Propene over Acidic Mordenites, *J. Catal.*, 1999, **185**, 131–137.

39 C. Bi, Z. Yao, X. Sun, X. Wei, J. Wang and J. Tian, Perovskite Quantum Dots with Ultralow Trap Density by Acid Etching-Driven Ligand Exchange for High Luminance and Stable Pure-Blue Light-Emitting Diodes, *Adv. Mater.*, 2021, **33**, 2006722.

40 Q. Zhong, M. Cao, Y. Xu, P. Li, Y. Zhang, H. Hu, D. Yang, Y. Xu, L. Wang, Y. Li, X. Zhang and Q. Zhang, L-Type Ligand-Assisted Acid-Free Synthesis of CsPbBr_3 Nanocrystals with Near-Unity Photoluminescence Quantum Yield and High Stability, *Nano Lett.*, 2019, **19**, 4151–4157.

41 H. Zhang, J. J. De Yoreo and J. F. Banfield, A Unified Description of Attachment-Based Crystal Growth, *ACS Nano*, 2014, **8**, 6526–6530.

42 D. Li, M. H. Nielsen, J. R. I. Lee, C. Frandsen, J. F. Banfield and J. J. De Yoreo, Direction-Specific Interactions Control Crystal Growth by Oriented Attachment, *Science*, 2012, **336**, 1014–1018.

43 S. Bhaumik, Oriented Attachment of Perovskite Cesium Lead Bromide Nanocrystals, *ChemistrySelect*, 2019, **4**, 4538–4543.

44 L. Peng, A. Dutta, R. Xie, W. Yang and N. Pradhan, Dot-Wire-Platelet-Cube: Step Growth and Structural Transformations in CsPbBr_3 Perovskite Nanocrystals, *ACS Energy Lett.*, 2018, **3**, 2014–2020.

45 J. Liu, K. Song, Y. Shin, X. Liu, J. Chen, K. X. Yao, J. Pan, C. Yang, J. Yin, L.-J. Xu, H. Yang, A. M. El-Zohry, B. Xin, S. Mitra, M. N. Hedhili, I. S. Roqan, O. F. Mohammed, Y. Han and O. M. Bakr, Light-Induced Self-Assembly of Cubic CsPbBr_3 Perovskite Nanocrystals into Nanowires, *Chem. Mater.*, 2019, **31**, 6642–6649.

46 J. T. DuBose, A. Christy, J. Chakkamalayath and P. V. Kamat, Transformation of Perovskite Nanoplatelets to Large Nanostructures Driven by Solvent Polarity, *ACS Mater. Lett.*, 2021, **4**, 93–101.